

pubs.acs.org/NanoLett Letter

# Dissipation from Interlayer Friction in Graphene Nanoelectromechanical Resonators

Paolo F. Ferrari, SunPhil Kim, and Arend M. van der Zande\*



Cite This: Nano Lett. 2021, 21, 8058-8065



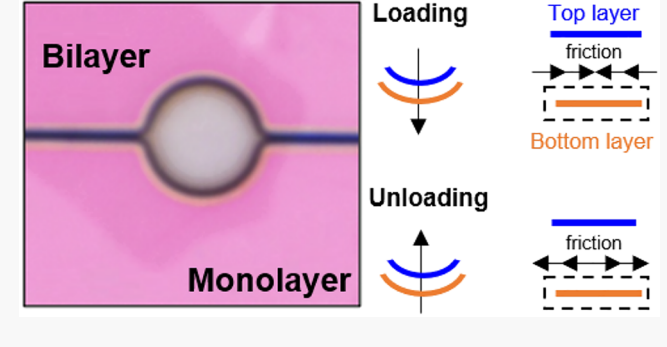
**ACCESS** 

Metrics & More



Supporting Information

ABSTRACT: A unique feature of two-dimensional (2D) materials is the ultralow friction at their van der Waals interfaces. A key question in a new generation of 2D heterostructure-based nanoelectromechanical systems (NEMS) is how the low friction interfaces will affect the dynamic performance. Here, we apply the exquisite sensitivity of graphene nanoelectromechanical drumhead resonators to compare the dissipation from monolayer, Bernalstacked bilayer, and twisted bilayer graphene membranes. We find a significant difference in the average quality factors of three resonator types: 53 for monolayer, 40 for twisted and 31 for Bernal-stacked membranes. We model this difference as a combination of change in stiffness and additional dissipation



from interlayer friction during motion. We find even the lowest frictions measured on sliding 2D interfaces are sufficient to alter dissipation in 2D NEMS. This model provides a generalized approach to quantify dissipation in NEMS based on 2D heterostructures which incorporate interlayer slip and friction.

KEYWORDS: graphene, resonator, NEMS, friction, superlubricity

A major drawback in shrinking down mechanical components to the nanoscale is the excessive dissipation coming from friction at sliding interfaces. Indeed, a long sought capability for micro- and nano-electromechanical systems (MEMS/ NEMS) is to incorporate structural lubricity to drastically reduce friction. 1,2 The 2D materials are promising candidantes to solve this challenge, where structural lubricity arises from the weak van der Waals interaction when layers are misaligned or have different lattice constants.<sup>3–9</sup> Integration of ultralow friction van der Waals interfaces with MEMS would unlock a new generation of dynamically slippable microsystems 10-12 and reconfigurable interfaces. 13-17 More generally, 2D materials have enormous potential in NEMS applications due to their diverse electronic and optical properties, mechanical stability, and ultrasmall size. <sup>18-33</sup> Indeed, 2D NEMS demonstrate high tunability at MHz/GHz frequencies, 22,25,27,34 high sensitivity, <sup>26,28,29</sup> and coupling to intrinsic material phenomena. <sup>30,32,33</sup> Constructing 2D heterostructures for 2D NEMS enables capabilities not available to a single material,<sup>35</sup> where different layers may act as electrodes, 36 isolate airsensitive materials, or incorporate superconductivity<sup>37</sup> and magnetism.<sup>30</sup> Yet, one of the primary metrics limiting the performance of 2D NEMS for real applications is their low quality factor (high dissipation). <sup>18,24</sup> Thus, a key question both for understanding the performance of 2D resonators and the emerging class of slippable systems is how interlayer friction affects the energy dissipation during dynamic motion.

Dissipation, or quality factor (*Q*), is one of the most critical properties determining performance in NEMS, yet the most difficult to design or control. Due to scaling laws, as the size of a mechanical system decreases, the losses become more important compared with the energy stored within the resonator.<sup>38</sup> This becomes especially relevant in the case of 2D NEMS, as they represent the ultimate limit in thickness of mechanical membranes. Typical values at room temperature range from 10 to 1000<sup>18,39</sup> while at low temperatures are 10<sup>3</sup>–10<sup>5</sup>. Dissipation in monolayer 2D NEMS occurs as a result of several mechanisms, including viscous damping, dege dissipation, Ohmic losses, and nonlinear motion dege dissipation, and nonlinear entropic fluctuations.

One particular mystery in 2D resonators is that the measured quality factors do not significantly improve as thickness increases to a few layers <sup>18,39</sup> against expectations from theoretical scaling laws. This suggests that there are additional mechanisms of dissipation in multilayer 2D materials, occurring as a result of the weak bonding and out of plane shear modulus of the van der Waals interface. <sup>53–56</sup> For

Received: June 17, 2021
Revised: September 21, 2021
Published: September 24, 2021





instance, in the elastic regime, Raman spectroscopy of stacked 2D layers show ultralow frequency Terahertz shear modes. <sup>57,58</sup> Beyond the elastic regime, plastic slip between aligned layers leads to mobile stacking faults called solitons, which glide through the interface. <sup>59–61</sup> In twisted multilayers or heterostructures, the misalignment between layers leads to a moiré superlattice with no stable equilibrium for most angles <sup>62</sup> and structural lubricity. <sup>4,54</sup> What is not yet studied or understood is how the interlayer friction observed in previous measurements will affect the dynamic dissipation in 2D NEMS.

In this study, we utilize the exquisite sensitivity of 2D NEMS to probe the mechanics of both twisted and commensurate single van der Waals interfaces. We directly compare the resonances of nanoelectromechanical drumhead resonators from CVD grown monolayer graphene (ML), Bernal-stacked bilayer graphene (BS-BL), and twisted bilayer graphene (T-BL). We observe a 30 and 70% higher dissipation factors  $(Q^{-1})$ in the twisted and Bernal-stacked bilayer resonators (respectively) versus the monolayer resonators. We build a model to explain the additional dissipation as a new form of internal friction unique to 2D NEMS rising from the interlayer friction and slip between the layers. The interlayer friction and interlayer slip leads to hysteresis in stress and strain during resonance. We apply the model to show that the range of friction from incommensurate twisted bilayers is sufficient to significantly alter dissipation. In commensurate bilayers, we find that even small numbers of solitons lead to similar or even larger dissipation. These models provide a guide to design NEMS from 2D heterostructures.

Figure 1a shows a schematic of the structure of the graphene drumhead resonator with the electrical circuit for actuation. Figure 1b shows an optical image of a typical resonator from twisted bilayer graphene. To fabricate the 2D drumhead resonators, we transfer and suspend 2D atomic membranes composed of twisted bilayer graphene (T-BL), Bernal-stacked bilayer graphene (BS-BL), and monolayer graphene (ML) over arrays of circular holes with 5  $\mu$ m diameter and 250 nm depth in a 285 nm thick silicon oxide layer on a degenerately doped silicon substrate.60 We electrically contact the transferred layer by evaporating Cr/Au 5/40 nm through a shadow mask. We use chemical vapor deposition grown graphene, which results in bilayer patches 20-40  $\mu$ m in size on a continuous monolayer. Using as-grown bilayers ensures the interface is clean without any residue that could result from the sequential transfer of layers. The CVD graphene bilayer patches naturally occur with both aligned and twisted stacking orientations. To confirm the stacking orientation in bilayer graphene membranes, we use Raman spectroscopy and compare the ratio of the graphene G/2D peaks.<sup>63</sup> Figure 1c shows the Raman spectra of ML (blue line), BS-BG (red line), and T-BLG (green line) at the indicated positions in Figure 1b. The monolayer shows a typical graphene Raman spectra with a Lorentzian shape of the 2D peak with FWHM =  $28.6 \text{ cm}^{-1}$  and a 2:1 ratio of 2D to G peak intensities. In contrast, the twisted bilayer shows a significant 4:1 enhancement in 2D band intensity and a narrower 2D peak width, typical of bilayer stacking with twist angle  $\theta > 16^{\circ}$ . Supporting Information Section S1 contains additional info on sample fabrication and measurement methods.

To study the mechanics of the van der Waals interface, we compare the mechanical drumhead resonance of the different membrane types. Figure 1d plots a typical mechanical response versus drive frequency of the first fundamental drumhead

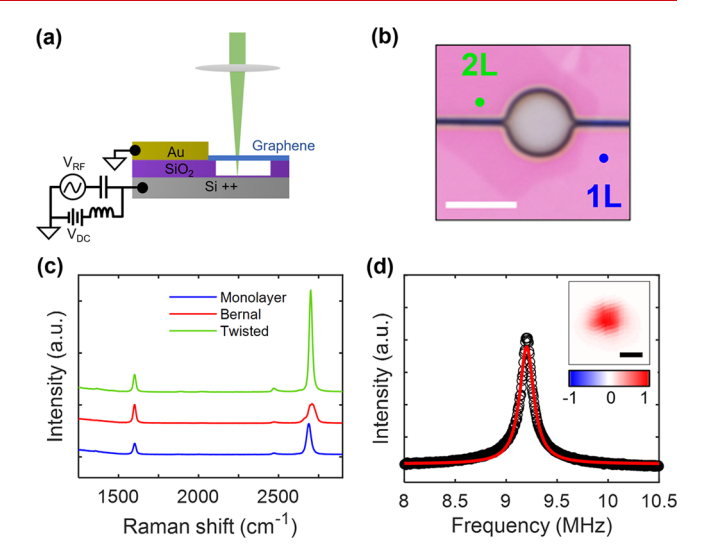


Figure 1. Structure of bilayer graphene drumhead resonator. (a) Schematic of a suspended 2D membrane drumhead resonator and the electronic actuation and optical detection scheme. The suspended membrane is electrostatically actuated while the mechanical motion is detected via Fabry-Pérot interferometry. (b) An optical image of suspended twisted bilayer graphene drumhead. Monolayer and twisted bilayer regions are indicated by blue and green dots, respectively. Circular membrane diameter and scale bar is 5  $\mu$ m. Small trenches on left and right prevent trapping of gas or residue during fabrication. (c) Raman spectra of monolayer graphene (blue), Bernal-stacked bilayer graphene (red), and twisted bilayer graphene (green). The blue and green dots in (b) indicate the measurement locations corresponding to the monolayer and twisted spectra. (d) First fundamental resonance of the resonator at (b) using  $\overline{V}_{DC} = 2 \text{ V}$ , Laser power = 50  $\mu$ W. Inset: Amplitude mapping at f = 9.2 MHz showing the fundamental mode. Scale bar = 2  $\mu$ m.

mode in the twisted bilayer graphene membrane shown in Figure 1b, using the scheme shown in Figure 1a. The inset shows the measured eigenmode of the resonance, confirming it is the fundamental drumhead mode. For the resonance measurements, we electrostatically actuate the membranes by applying a DC voltage  $V_{\rm DC}$  with respect to the silicon substrate to tension the membranes and an RF voltage  $V_{\mathrm{RF}}$  to drive the resonance. We detect the mechanical resonance via the dynamic reflectance of a laser spot focused on the membrane, which changes as the membrane moves due to a change in the optical interference between the membrane and silicon gate. 18,64,65 All measurements are performed in high vacuum with  $P < 10^{-6}$  Torr. In the linear regime, the resonance of the bilayer membrane is well described by a Lorentzian fit (red line) with resonance frequency of f = 9.2 MHz and full width half-maximum (FWHM)  $\Delta f$  = 161 kHz when driven at  $V_{\rm DC}$  = 2 V and  $V_{RF}$  = 35 mV and measured with incident laser power  $P = 50 \mu W$ . Dissipation in resonators is typically represented as either the dissipation rate  $\Gamma = 2\pi\Delta f$  or the quality factor Q = $\omega/\Gamma = f_0/\Delta f$ . In the linear regime for this device, Q = 57 and  $\Gamma$ = 1005 kHz. Supporting Information Figures S1-S3 compare the linear and nonlinear resonance response and electrostatic tuning for all membrane types.

Before comparing the dynamics, we first evaluate the impact of the different interfaces on the morphology of the membranes. Figure 2 compares both optical images (a–d) and the topography (e–h) measured using atomic force microscopy (AFM) of four different types of resonators, (a,e) monolayer graphene (ML), (b,f) Bernal-stacked bilayer

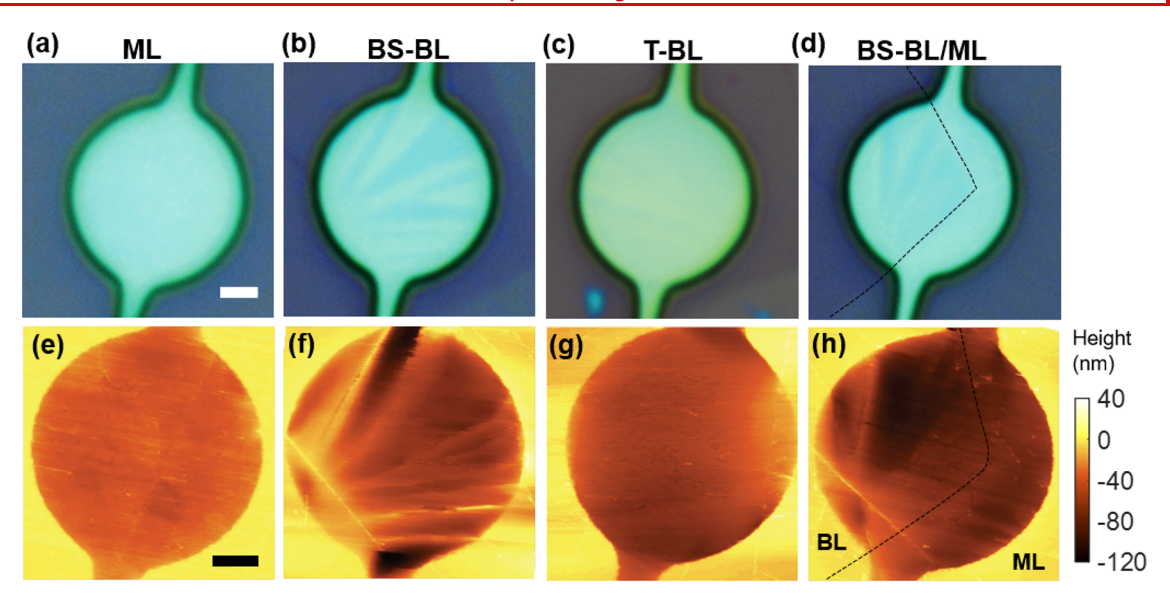
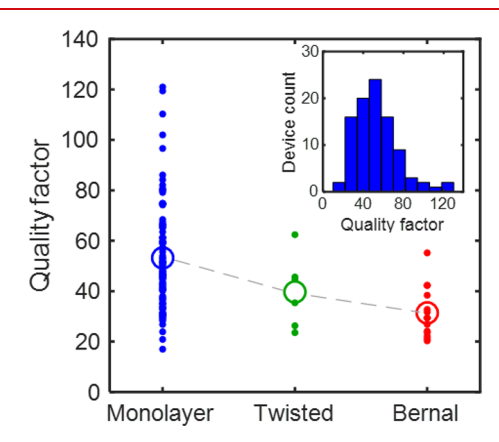


Figure 2. Morphology of graphene membranes. On the top, optical images of (a) monolayer, (b) Bernal-stacked bilayer, (c) twisted bilayer, and (d) half monolayer and half Bernal-stacked bilayer. On the bottom (e-h), atomic force microscopy (AFM) topographic maps of the same membranes. On (d,f), the dashed line indicates the monolayer-bilayer boundary. We note that the similar position of a ripple in the bottom left regions of the resonators at (f,h) are purely coincidental. Scale bars = 1  $\mu$ m.

graphene (BS-BL), (c,g) twisted bilayer graphene (T-BL), and (d,h) a membrane that is part Bernal stacked bilayer and part monolayer. Both ML as well as T-BL resonators have a flat surface with ripples only up to 10 nm in height. Changes in topography observed in AFM are visible as changes in contrast optically due to interference. In contrast, the BS-BL resonators have ripples that are ~100-500 nm wide and 10-100 nm high. Interestingly, this same pattern is observed in Figure 2d,h where the bilayer region is buckled, whereas the monolayer region is relatively flat. The same pattern occurs in all other samples, and we have previously observed the same behavior. The presence of the ripples in the BS-BL resonators are consistent with kink and antikink defect rising from local stacking faults known as solitons.<sup>60</sup> The competition between in-plane strain, stacking-fault energy, and bending result in the buckled geometry that is seen in the BS-BL membranes but not in the monolayer or twisted samples.

A challenge of 2D resonators and NEMS in general is that they are sensitive to variations in pretension, surface contaminants, added mass, potential grain boundaries, clamping, and membrane morphology, which lead to large and difficult to control device-to-device variations in dissipation and frequency. 20,66,67 Thus, it is not advisible to infer universal behavior from single devices. Instead, it is necessary to take a statistical analysis of behavior. Figure 3 shows the spread in quality factors for many otherwise identical resonators on a single substrate made from monolayer, twisted bilayer, and Bernal-stacked bilayer graphene, respectively. The inset of Figure 3 is a histogram of the quality factors for just the monolayers, showing a total of 95 devices measured. Similarly, we measured a total of 14 Bernal stacked bilayers, and 6 twisted bilayers on the same substrate. The relative number of devices measured are due to the lower occurrence of bilayers and the even lower occurrence of twisted bilayers versus Bernal-stacked bilayers. For all measurements, we choose identical parameters to those shown in Figure 1d, and confirm that all devices are operating in the linear regime. Shown in Supporting Information Figure S2, all resonator types show similar eigenmodes despite the differ-



**Figure 3.** Measured quality factors of the three types of resonators on Substrate 1 for monolayer (blue), twisted bilayer (green), and Bernalstacked bilayer (red). The empty circles indicate the statistical average and a dashed line connects the averages for comparison. Inset: Histogram of the monolayer quality factors for Substrate 1.

ences in morphology. We exclude from our analysis any resonators with obvious defects, such as tears, folds, large particles, or holes and only included resonances which show the fundamental eigenmode profile.

While there is a large range in measured values, on average monolayer graphene has a larger quality factor (smaller dissipation)  $\langle Q^{\text{ML}} \rangle = 53.2 \pm 20.8$ , followed by the twisted bilayer  $\langle Q^{\text{T-BL}} \rangle = 40 \pm 12.2$  and the Bernal-stacked bilayer devices  $\langle Q^{\text{BS-BL}} \rangle = 31 \pm 9.7$ . Supporting Information Figure S4 shows a similar trend in the FWHM  $\Delta f$ . Supporting Information Figure S5 shows that similar trends for the quality factor occur on other substrates measured, although the average values are different, likely due to different pretension and contamination rising from small variations in synthesis and processing. On average, both types of bilayer resonators showed higher dissipation factors than monolayer in the linear regime: 30% higher for twisted and 70% higher for the Bernal-stacked cases, which indicates the presence of an additional linear dissipation channel. However, an important question is

how much of the change in quality factor is due to a change in stiffness versus a change in dissipation. To address this question, Supporting Information Figure S4 shows the statistical frequency analysis. There is no observable correlation between the frequency and the quality factor. On average, the resonance frequency of monolayers is 15.1 MHz, whereas both Bernal-stacked bilayers and twisted bilayers are 12.6 MHz. This means that there is a 17% lower frequency or stiffness in the bilayers versus monolayers, which should cause a 17% difference in the quality factor from the change in stored energy. We attribute the remaining change in measured quality factor to a change in dissipation.

Generally, dissipation in mechanical resonators rises from multiple mechanisms operating in parallel, and it is difficult to pin down the dominant mechanism. For example, there have been important studies of monolayer graphene dissipation, via entropic motion and nonlinear mechanics, 46,48,49,51,52 and systematic studies of strain, electrostatic tuning, membrane size and thickness have shown all play a role. 39,66,68,69 However, the exact mechanisms are still not understood, especially at room temperature. This study does not attempt to address the origin of all types of graphene dissipation and instead focuses only on the new sources of dissipation rising from interfacial mechanics. We propose a model to explain the extra dissipation as arising from friction between the layers. This model is a nanoscale analog to established structural or slip damping models used to quantify dissipation in macroscopic systems. 70,71 Structural damping is frequently applied in systems where slip and friction change the stress in slightly compliant mechanisms. The end result is a hysteresis loop in stress and strain which leads to work lost during cyclic motion. This behavior is a special subcase of the more general form of dissipation from internal friction rising from defects and interfaces in materials and often found in MEMS and NEMS.<sup>38</sup> Structural damping is a linear mechanism and should not be mistaken for the similar nonlinear mechanism, Coulomb damping, which models friction and slip in rigid systems. In Supporting Information Section S2d, we also estimate the impact of ripples seen in the Bernal-stacked resonators on other common mechanisms, including thermoelastic and nonlinear dissipation, and show they do not significantly contribute to overall dissipation.

Figure 4a shows the nanoscale view of interlayer stress in bilayer graphene resonators during motion. Figure 4b shows the equivalent lumped element model describing the behavior, where the bottom layer acts as a dissipative mass-spring system weakly coupled via friction to the top layer. The dissipation in the bottom layer represents all mechanisms except those coming from the interaction between the layers. For simplicity, we assume that the bottom layer (shown in orange) is well clamped on the substrate, leading to small variations in the local stress as the membrane moves. Essentially, the bottom layer responds in exactly the same manner as a monolayer membrane. In contrast, the top layer (shown in blue) is only weakly clamped and interacts primarily with the bottom layer, not with the substrate. As a result, atomic-scale slip between layers occurs whenever the dynamic stress induced in the bottom layer is enough to overcome the friction  $\sigma_{\rm f}$ . The interlayer friction  $\sigma_{\rm f}$  is the induced stress in the bottom membrane, expressed in units of N/m. Figure 4c and d show the resulting stress-strain cycle for an arbitrary point in the bottom (orange) and top (blue) layers, respectively. Before resonance, the layers are in equilibrium with a similar but not

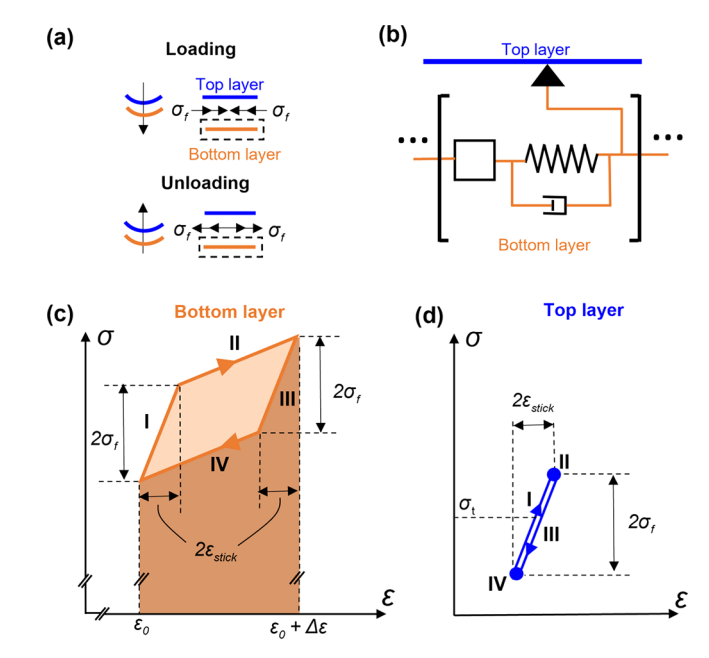


Figure 4. Schematics of the proposed friction model. (a) Overall view of the action of interlayer friction  $\sigma_{\rm f}$  on the bottom layer during the loading (top) and unloading (bottom) parts of an oscillation cycle. (b) Equivalent lumped-element model. The electrostatic force exerts tension in the bottom layer, which we model as a series of mass, spring and dashpot elements, coupled via friction with the top layer. (c,d) Schematic picture of the stress–strain relationship of the bottom (c) and top layer (d) during an oscillation cycle, shown as a series of paths (I–IV).

necessarily equal stress/strain, leading to some static 3D deflection. In the loading (unloading) part of a cycle, friction will exert a compressive (tensile) stress  $-\sigma_{\rm f}$  ( $+\sigma_{\rm f}$ ) on the bottom layer, leading to a hysteresis loop in the stress with an amplitude  $2\sigma_{\rm f}$ . If there were perfect elastic coupling between the layers with no slip, the membrane would transfer strain through elastic shear and there would be no hysteresis loop.

The cycle of resonance leads to a hysteresis loop with four steps. (I–II) Initially, the strain/stress in the bottom layer is elastically transmitted into the top layer until the applied force in the bottom layer overcomes the tensile interlayer friction. During this step, both layers deform by  $2\epsilon_{\rm stick}$  , where  $\epsilon_{\rm stick}$  is the "stick" component of the strain. The strain and stress in the top layer increase linearly until the stress reaches  $\sigma_t + \sigma_{tr}$  where  $\sigma_t$  is the initial stress in the top layer. In both layers, the stress increases by  $2\sigma_f$  during this step. (II-III) After the friction barrier is overcome, the layers slip until loading is reversed. The stress in the top layer will stay constant at  $\sigma_t + \sigma_f$ . The stress in the bottom layer will increase linearly with a slope equal to the Young's modulus of monolayer graphene. (III-IV) Similarly, during initial unloading the interlayer friction prevents slip between the layers until the compressive friction barrier is overcome. The stress in the top layer will decrease linearly to  $\sigma_{\rm t} - \sigma_{\rm f}$ . The strain variation in both layers is the same as before (2 $\epsilon_{
m stick}$ ), while the stress decreases by 2 $\sigma_{
m f}$  (IV– I) Finally, for additional unloading the bottom layer slips again relative to the top layer until the cycle is completed.

Just as with any lumped element model, these calculations represent an effective or average behavior. In any real system, the slip and movement of atoms during resonance will be inhomogeneous (in incommensurate systems) or localized to a few defects (in solitons), thus friction forces will have a

stochastic nature.<sup>4,72</sup> Our model describes the equivalent dynamics by assuming it is evenly distributed over the entire interface and does not reveal the dynamics of any single defect. Similar assumptions are frequently made in tribology and internal friction models of damping. To calculate the total influence of friction on the graphene resonator, we numerically calculate the stored and dissipated energy for the first eigenmode using finite element simulations. The full derivations, assumptions, and methodology for the simulations are provided in Supporting Information Section S2 and Figure S6. In the Supporting Information, we do a general analysis including both stick and slip components and find that the stick component of the deformation is essentially zero for the range of values relevant to 2D resonators. As a result, for the analysis below we only consider the pure slip case  $\epsilon_{\rm stick} = 0$ .

Figure 5 is a parametric analysis of the effective quality factor of bilayer graphene as a function of interlayer friction, initial stress, and initial quality factor. Figure 5a plots the effective bilayer quality factor versus the log of interlayer friction, at

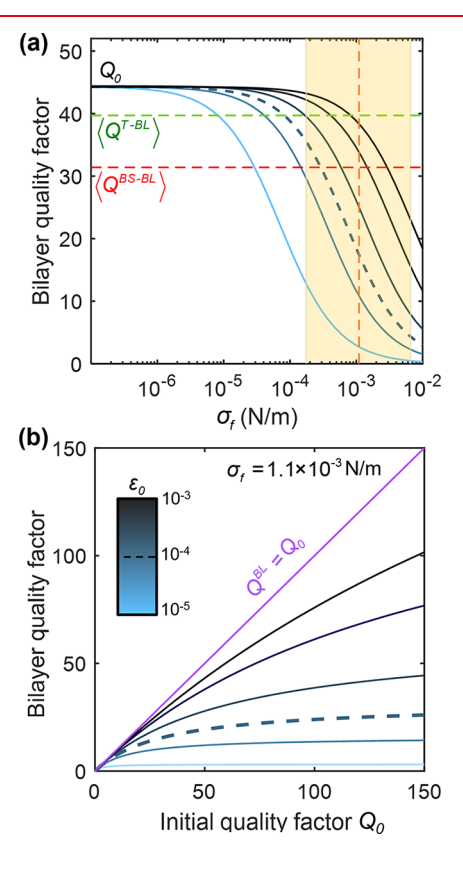


Figure 5. Parametric analysis of bilayer quality factors predicted by the slip model. (a) Plot of bilayer quality factor versus interlayer friction  $\sigma_{\rm f}$  for different prestrains  $\epsilon_0=10^{-5}-10^{-3}$ . Color scale shown on (b). The dashed blue line indicates the typical value of  $\epsilon_0=10^{-4}$ . For reference, the horizontal lines indicate the average quality factors for twisted bilayer (green) and Bernal-stacked bilayer (red) from Figure 3. We assume the average quality factor of monolayer (black) as the unperturbed quality factor in the model to generate the plot. The shaded yellow area represents the range of expected friction stress and its average (dashed orange line) obtained from tribological measurements. (b) Plot of bilayer quality factor versus initial quality factor for the same range of prestrains shown in (a). We assume a fixed interlayer friction of  $\sigma_{\rm f}=1.1\times10^{-3}~{\rm N/m}$ , corresponding with the orange line in (a). For comparison, the purple line indicates the case of no friction,  $Q^{\rm BL}=Q_0$ .

different levels of prestrain (color bar shown in Figure 5b). In this plot, the frictionless bilayer quality factor is assumed to be  $Q_0 = 44.4$ , the amplitude of motion at the midpoint is 0.2 nm, and the range of prestrains spans the values previously measured by our group and others on devices with the same geometry and fabrication steps. 60 The horizontal bands on the plot compare the average quality factors for the two measured bilayer cases, twisted (green) and Bernal stacked (red). As a comparison, the shaded yellow region shows the range of interlayer frictions measured statically in graphite interfaces,<sup>72</sup> along with the average of  $\sigma_f = 1.1 \times 10^{-3} \text{ N/m}$  (dashed orange line). We tabulate other experimental estimates of  $\sigma_{\rm f}$  from the literature in Supporting Information Section S3, and show that they qualitatively agree. From Figure 5a, as expected, at very low frictions there is essentially no influence of friction on quality factor. Under higher friction, the quality factor drops drastically. The comparisons reveal that the interlayer friction is of sufficient magnitude to drastically change the quality factor but not enough to overdamp the resonance.

Figure 5b shows the effect of different initial quality factors  $Q_0$  on the value of Q obtained for a fixed interlayer friction of  $\sigma_{\rm f}=1.1\times 10^{-3}$  N/m, at different levels of prestrain (inset color bar). As expected, the impact of friction becomes more pronounced at higher initial quality factors. This observation explains the spread of Q seen in Figure 3 and Supporting Information Figure S5, where the range of quality factors for monolayer has a much larger tail than the twisted or Bernalstacked cases. Because higher quality factor resonators are more strongly impacted by friction, any spread in values will be suppressed by friction.

Here, we showed that interlayer friction plays a significant role in the dissipation of both twisted and Bernal-stacked bilayer graphene resonators. In both cases, dynamic interlayer stress induced slip between the layers causes an additional dissipation source compared to monolayer. For the twisted bilayer resonators, friction is associated with the superlubric interface where the moiré superlattice leads to an even distribution in atoms rearranging with very low energy barriers. For the Bernal-stacked case, friction is a result of a small number of local stacking faults gliding and rearranging <sup>59</sup> with each having a relatively large contribution. In both cases, these local rearrangements are inelastic, which leads to the hysteresis in stress and strain and added dissipation.

This study outlines an alternative method of measuring friction in 2D materials which allows tuning and probing of parameters difficult to access via traditional nanotribology approaches, such as varying temperature, interfacial stress or probing internal van der Waals interfaces in multilayer heterostructures. For example, future studies include fundamental studies of friction and superlubricity by measuring dissipation at cryogenic temperatures. Moreover, structural lubricity is a long sought capability in MEMS because it opens access to a host of new device concepts otherwise precluded by scaling laws such as slip-based switches and rotors. Recent proposed systems actively utilize slippable interfaces for switching <sup>12,72</sup> or to dynamically reconfigure electronic properties. <sup>13,14,16,17</sup> Our model for the role of slip on dissipation will be critical to the design and determining ultimate performance in these systems.

### ASSOCIATED CONTENT

# Supporting Information

The Supporting Information is available free of charge at https://pubs.acs.org/doi/10.1021/acs.nanolett.1c02369.

Methods of sample fabrication, characterization, and measurement; description of model and simulation methods; comparison to previous friction literature. Figures S1-S8: (S1) drive dependence of amplitude and quality factor for characteristics of three representative devices (monolayer, twisted and Bernal-stacked graphene); (S2) eigenmode mapping for representative devices of the three resonator types; (S3) Electrostatic tuning of frequency and quality factor of a representative device; (S4) frequency, FWHM, and quality factor data of all devices in Substrate 1; (S5) quality factor of all devices in Substrates 1, 2, and 3; (S6) picture of the membrane's FEA model; (S7) dependence of the calculated quality factor on amplitude of motion; (S8) plot of quality factor versus amplitude considering stick and slip components of strain (PDF)

#### AUTHOR INFORMATION

#### **Corresponding Author**

Arend M. van der Zande — Department of Mechanical Science and Engineering, University of Illinois at Urbana—Champaign, Urbana, Illinois 61801, United States; Materials Research Laboratory, University of Illinois at Urbana—Champaign, Urbana, Illinois 61801, United States; orcid.org/0000-0001-5104-9646; Email: arendv@illinois.edu

## **Authors**

Paolo F. Ferrari — Department of Mechanical Science and Engineering, University of Illinois at Urbana—Champaign, Urbana, Illinois 61801, United States; orcid.org/0000-0001-9787-553X

SunPhil Kim — Department of Mechanical Science and Engineering, University of Illinois at Urbana—Champaign, Urbana, Illinois 61801, United States; ocid.org/0000-0002-5627-1139

Complete contact information is available at: https://pubs.acs.org/10.1021/acs.nanolett.1c02369

## **Author Contributions**

P.F.F. and SP. K. fabricated the samples and performed the measurements under the supervision of A.v.d.Z. P.F.F. and A.v.d.Z developed the model and P.F.F. performed the FEA simulations under the supervision of A.v.d.Z. All authors discussed the results and read and contributed to the manuscript.

#### Notes

The authors declare no competing financial interest.

## ACKNOWLEDGMENTS

This work was supported by the NSF-CAREER Award, number CMMI-1846732. This work was carried out in part in the Holonyak Micro and Nano Technology Laboratory (HMNTL) and the Materials Research Laboratory (MRL) Central Facilities. The authors acknowledge the use of facilities and instrumentation supported by the NSF through the University of Illinois Materials Research Science and Engineering Center award number DMR-1720633.

## **■** REFERENCES

- (1) Hod, O.; Meyer, E.; Zheng, Q.; Urbakh, M. Structural superlubricity and ultralow friction across the length scales. *Nature* **2018**, *563*, 485–492.
- (2) Vanossi, A.; Bechinger, C.; Urbakh, M. Structural lubricity in soft and hard matter systems. *Nat. Commun.* **2020**, *11*, 4657.
- (3) Martin, J. M.; Donnet, C.; Le Mogne, T.; Epicier, T. Superlubricity of molybdenum disulphide. *Phys. Rev. B: Condens. Matter Mater. Phys.* **1993**, 48, 10583–10586.
- (4) Dienwiebel, M.; Verhoeven, G. S.; Pradeep, N.; Frenken, J. W. M.; Heimberg, J. A.; Zandbergen, H. W. Superlubricity of Graphite. *Phys. Rev. Lett.* **2004**, *92*, 126101.
- (5) Liu, Z.; Yang, J.; Grey, F.; Liu, J. Z.; Liu, Y.; Wang, Y.; Yang, Y.; Cheng, Y.; Zheng, Q. Observation of Microscale Superlubricity in Graphite. *Phys. Rev. Lett.* **2012**, *108*, 205503.
- (6) Feng, X.; Kwon, S.; Park, J. Y.; Salmeron, M. Superlubric Sliding of Graphene Nanoflakes on Graphene. ACS Nano 2013, 7, 1718–1724
- (7) Song, Y.; Mandelli, D.; Hod, O.; Urbakh, M.; Ma, M.; Zheng, Q. Robust microscale superlubricity in graphite/hexagonal boron nitride layered heterojunctions. *Nat. Mater.* **2018**, *17*, 894–899.
- (8) Wang, W.; Shen, J.; He, Q.-C. Microscale superlubricity of graphite under various twist angles. *Phys. Rev. B: Condens. Matter Mater. Phys.* **2019**, 99, 054103.
- (9) Li, H.; Wang, J.; Gao, S.; Chen, Q.; Peng, L.; Liu, K.; Wei, X. Superlubricity between MoS2Monolayers. *Adv. Mater.* **2017**, 29, 1701474.
- (10) Mehregany, M.; Tai, Y.-C. Surface micromachined mechanisms and micromotors. *J. Micromech. Microeng.* **1991**, *1*, 73–85.
- (11) Garcia, E. J.; Sniegowski, J. J. Surface micromachined microengine. Sens. Actuators, A 1995, 48, 203–214.
- (12) Huang, X.; Xiang, X.; Nie, J.; Peng, D.; Yang, F.; Wu, Z.; Jiang, H.; Xu, Z.; Zheng, Q. Microscale Schottky superlubric generator with high direct-current density and ultralong life. *Nat. Commun.* **2021**, *12*, 2268.
- (13) Koren, E.; Leven, I.; Lörtscher, E.; Knoll, A.; Hod, O.; Duerig, U. Coherent commensurate electronic states at the interface between misoriented graphene layers. *Nat. Nanotechnol.* **2016**, *11*, 752–757.
- (14) Ribeiro-Palau, R.; Zhang, C.; Watanabe, K.; Taniguchi, T.; Hone, J.; Dean, C. R. Twistable electronics with dynamically rotatable heterostructures. *Science* **2018**, *361*, 690–693.
- (15) Finney, N. R.; Yankowitz, M.; Muraleetharan, L.; Watanabe, K.; Taniguchi, T.; Dean, C. R.; Hone, J. Tunable crystal symmetry in graphene—boron nitride heterostructures with coexisting moiré superlattices. *Nat. Nanotechnol.* **2019**, *14*, 1029–1034.
- (16) Yao, H.; Chen, C.; Xue, W.; Bai, F.; Cao, F.; Lan, Y.; Liu, X.; Wang, Y.; Singh, D. J.; Lin, X.; Zhang, Q. Enhanced tunable second harmonic generation from twistable interfaces and vertical superlattices in boron nitride homostructures. *Science Advances* **2021**, *7*, No. eabe8691.
- (17) Yu, J.; Hossain, M. A.; Kim, S.; Ferrari, P. F.; Huang, S.; Zhang, Y.; Kim, H.; Michel, D. A.; van der Zande, A. M. Mechanically sensing and tailoring electronic properties in two-dimensional atomic membranes. *Curr. Opin. Solid State Mater. Sci.* **2021**, *25*, 100900.
- (18) Bunch, J. S.; van der Zande, A. M.; Verbridge, S. S.; Frank, I. W.; Tanenbaum, D. M.; Parpia, J. M.; Craighead, H. G.; McEuen, P. L. Electromechanical Resonators from Graphene Sheets. *Science* **2007**, *315*, 490–493.
- (19) Chen, C.; Rosenblatt, S.; Bolotin, K. I.; Kalb, W.; Kim, P.; Kymissis, I.; Stormer, H. L.; Heinz, T. F.; Hone, J. Performance of monolayer graphene nanomechanical resonators with electrical readout. *Nat. Nanotechnol.* **2009**, *4*, 861–867.
- (20) Zande, A. M. v. d.; Barton, R. A.; Alden, J. S.; Ruiz-Vargas, C. S.; Whitney, W. S.; Pham, P. H. Q.; Park, J.; Parpia, J. M.; Craighead, H. G.; McEuen, P. L. Large-Scale Arrays of Single-Layer Graphene Resonators. *Nano Lett.* **2010**, *10*, 4869–4873.
- (21) Castellanos-Gomez, A.; van Leeuwen, R.; Buscema, M.; van der Zant, H. S. J.; Steele, G. A.; Venstra, W. J. Single-Layer MoS2Mechanical Resonators. *Adv. Mater.* **2013**, *25*, 6719–6723.

- (22) Chen, C.; Lee, S.; Deshpande, V. V.; Lee, G.-H.; Lekas, M.; Shepard, K.; Hone, J. Graphene mechanical oscillators with tunable frequency. *Nat. Nanotechnol.* **2013**, *8*, 923–927.
- (23) Zheng, X.-Q.; Lee, J.; Feng, P. X.-L. Hexagonal boron nitride nanomechanical resonators with spatially visualized motion. *Microsystems & Nanoengineering* **2017**, *3*, 17038.
- (24) van Leeuwen, R.; Castellanos-Gomez, A.; Steele, G. A.; van der Zant, H. S. J.; Venstra, W. J. Time-domain response of atomically thin MoS2 nanomechanical resonators. *Appl. Phys. Lett.* **2014**, *105*, 041911.
- (25) Ye, F.; Lee, J.; Feng, P. X. L. Electrothermally Tunable Graphene Resonators Operating at Very High Temperature up to 1200 K. *Nano Lett.* **2018**, *18*, 1678–1685.
- (26) Dolleman, R. J.; Davidovikj, D.; Cartamil-Bueno, S. J.; van der Zant, H. S. J.; Steeneken, P. G. Graphene Squeeze-Film Pressure Sensors. *Nano Lett.* **2016**, *16*, 568–571.
- (27) De Alba, R.; Massel, F.; Storch, I. R.; Abhilash, T. S.; Hui, A.; McEuen, P. L.; Craighead, H. G.; Parpia, J. M. Tunable phonon-cavity coupling in graphene membranes. *Nat. Nanotechnol.* **2016**, *11*, 741–746
- (28) Blaikie, A.; Miller, D.; Alemán, B. J. A fast and sensitive room-temperature graphene nanomechanical bolometer. *Nat. Commun.* **2019**, *10*, 4726.
- (29) Lemme, M. C.; Wagner, S.; Lee, K.; Fan, X.; Verbiest, G. J.; Wittmann, S.; Lukas, S.; Dolleman, R. J.; Niklaus, F.; van der Zant, H. S. J.; Duesberg, G. S.; Steeneken, P. G. Nanoelectromechanical Sensors Based on Suspended 2D Materials. *Research* **2020**, 2020, 1.
- (30) Jiang, S.; Xie, H.; Shan, J.; Mak, K. F. Exchange magneto-striction in two-dimensional antiferromagnets. *Nat. Mater.* **2020**, *19*, 1295–1299.
- (31) Dolleman, R. J.; Belardinelli, P.; Houri, S.; van der Zant, H. S. J.; Alijani, F.; Steeneken, P. G. High-Frequency Stochastic Switching of Graphene Resonators Near Room Temperature. *Nano Lett.* **2019**, 19, 1282–1288.
- (32) Li, H.-K.; Fong, K. Y.; Zhu, H.; Li, Q.; Wang, S.; Yang, S.; Wang, Y.; Zhang, X. Valley optomechanics in a monolayer semiconductor. *Nat. Photonics* **2019**, *13*, 397–401.
- (33) Šiškins, M.; Lee, M.; Mañas-Valero, S.; Coronado, E.; Blanter, Y. M.; van der Zant, H. S. J.; Steeneken, P. G. Magnetic and electronic phase transitions probed by nanomechanical resonators. *Nat. Commun.* **2020**, *11*, 2698.
- (34) Singh, R.; Sarkar, A.; Guria, C.; Nicholl, R. J.; Chakraborty, S.; Bolotin, K. I.; Ghosh, S. Giant Tunable Mechanical Nonlinearity in Graphene–Silicon Nitride Hybrid Resonator. *Nano Lett.* **2020**, *20*, 4659–4666
- (35) Kim, S.; Yu, J.; van der Zande, A. M. Nano-electromechanical Drumhead Resonators from Two-Dimensional Material Bimorphs. *Nano Lett.* **2018**, *18*, 6686–6695.
- (36) Lee, S.; Adiga, V. P.; Barton, R. A.; van der Zande, A. M.; Lee, G.-H.; Ilic, B. R.; Gondarenko, A.; Parpia, J. M.; Craighead, H. G.; Hone, J. Graphene Metallization of High-Stress Silicon Nitride Resonators for Electrical Integration. *Nano Lett.* **2013**, *13*, 4275–4279.
- (37) Will, M.; Hamer, M.; Müller, M.; Noury, A.; Weber, P.; Bachtold, A.; Gorbachev, R. V.; Stampfer, C.; Güttinger, J. High Quality Factor Graphene-Based Two-Dimensional Heterostructure Mechanical Resonator. *Nano Lett.* **2017**, *17*, 5950–5955.
- (38) Imboden, M.; Mohanty, P. Dissipation in nanoelectromechanical systems. *Phys. Rep.* **2014**, *534*, 89–146.
- (39) Lee, J.; Wang, Z.; He, K.; Shan, J.; Feng, P. X.-L. High Frequency MoS2 Nanomechanical Resonators. ACS Nano 2013, 7, 6086–6091.
- (40) Lee, J.; Wang, Z.; He, K.; Shan, J.; Feng, P. X.-L. Air damping of atomically thin MoS2 nanomechanical resonators. *Appl. Phys. Lett.* **2014**, *105*, 023104.
- (41) Garcia-Sanchez, D.; van der Zande, A. M.; Paulo, A. S.; Lassagne, B.; McEuen, P. L.; Bachtold, A. Imaging Mechanical Vibrations in Suspended Graphene Sheets. *Nano Lett.* **2008**, *8*, 1399–1403.

- (42) Takamura, M.; Okamoto, H.; Furukawa, K.; Yamaguchi, H.; Hibino, H. Energy Dissipation in Graphene Mechanical Resonators with and without Free Edges. *Micromachines* **2016**, *7*, 158.
- (43) Seoánez, C.; Guinea, F.; Castro Neto, A. H. Dissipation in graphene and nanotube resonators. *Phys. Rev. B: Condens. Matter Mater. Phys.* **2007**, *76*, 125427.
- (44) Morell, N.; Reserbat-Plantey, A.; Tsioutsios, I.; Schädler, K. G.; Dubin, F.; Koppens, F. H. L.; Bachtold, A. High Quality Factor Mechanical Resonators Based on WSe2Monolayers. *Nano Lett.* **2016**, 16, 5102–5108
- (45) Eichler, A.; Moser, J.; Chaste, J.; Zdrojek, M.; Wilson-Rae, I.; Bachtold, A. Nonlinear damping in mechanical resonators made from carbon nanotubes and graphene. *Nat. Nanotechnol.* **2011**, *6*, 339.
- (46) Midtvedt, D.; Croy, A.; Isacsson, A.; Qi, Z.; Park, H. S. Fermi-Pasta-Ulam Physics with Nanomechanical Graphene Resonators: Intrinsic Relaxation and Thermalization from Flexural Mode Coupling. *Phys. Rev. Lett.* **2014**, *112*, 145503.
- (47) Güttinger, J.; Noury, A.; Weber, P.; Eriksson, A. M.; Lagoin, C.; Moser, J.; Eichler, C.; Wallraff, A.; Isacsson, A.; Bachtold, A. Energy-dependent path of dissipation in nanomechanical resonators. *Nat. Nanotechnol.* **2017**, *12*, 631–636.
- (48) De, S.; Kunal, K.; Aluru, N. R. Nonlinear intrinsic dissipation in single layer MoS2 resonators. *RSC Adv.* **2017**, *7*, 6403–6410.
- (49) De, S.; van der Zande, A.; Aluru, N. R. Intrinsic Dissipation Due to Mode Coupling in Two-Dimensional-Material Resonators Revealed Through a Multiscale Approach. *Phys. Rev. Appl.* **2020**, *14*, 034062.
- (50) Keşkekler, A.; Shoshani, O.; Lee, M.; van der Zant, H. S. J.; Steeneken, P. G.; Alijani, F. Tuning nonlinear damping in graphene nanoresonators by parametric—direct internal resonance. *Nat. Commun.* **2021**, *12*, 1099.
- (51) Barnard, A. W.; Sazonova, V.; van der Zande, A. M.; McEuen, P. L. Fluctuation broadening in carbon nanotube resonators. *Proc. Natl. Acad. Sci. U. S. A.* **2012**, *109*, 19093–19096.
- (52) Miao, T.; Yeom, S.; Wang, P.; Standley, B.; Bockrath, M. Graphene Nanoelectromechanical Systems as Stochastic-Frequency Oscillators. *Nano Lett.* **2014**, *14*, 2982–2987.
- (53) Kim, S. Y.; Park, H. S. Multilayer friction and attachment effects on energy dissipation in graphene nanoresonators. *Appl. Phys. Lett.* **2009**, *94*, 101918.
- (54) Wang, G.; Dai, Z.; Xiao, J.; Feng, S.; Weng, C.; Liu, L.; Xu, Z.; Huang, R.; Zhang, Z. Bending of Multilayer van der Waals Materials. *Phys. Rev. Lett.* **2019**, *123*, 116101.
- (55) Han, E.; Yu, J.; Annevelink, E.; Son, J.; Kang, D. A.; Watanabe, K.; Taniguchi, T.; Ertekin, E.; Huang, P. Y.; van der Zande, A. M. Ultrasoft slip-mediated bending in few-layer graphene. *Nat. Mater.* **2020**, *19*, 305–309.
- (56) Yu, J.; Han, E.; Hossain, M. A.; Watanabe, K.; Taniguchi, T.; Ertekin, E.; Zande, A. M.; Huang, P. Y. Designing the Bending Stiffness of 2D Material Heterostructures. *Adv. Mater.* **2021**, 33, 2007269.
- (57) Tan, P. H.; Han, W. P.; Zhao, W. J.; Wu, Z. H.; Chang, K.; Wang, H.; Wang, Y. F.; Bonini, N.; Marzari, N.; Pugno, N.; Savini, G.; Lombardo, A.; Ferrari, A. C. The shear mode of multilayer graphene. *Nat. Mater.* **2012**, *11*, 294–300.
- (58) Cong, C.; Yu, T. Enhanced ultra-low-frequency interlayer shear modes in folded graphene layers. *Nat. Commun.* **2014**, *5*, 4709.
- (59) Alden, J. S.; Tsen, A. W.; Huang, P. Y.; Hovden, R.; Brown, L.; Park, J.; Muller, D. A.; McEuen, P. L. Strain solitons and topological defects in bilayer graphene. *Proc. Natl. Acad. Sci. U. S. A.* **2013**, *110*, 11256–11260.
- (60) Kim, S.; Annevelink, E.; Han, E.; Yu, J.; Huang, P. Y.; Ertekin, E.; van der Zande, A. M. Stochastic Stress Jumps Due to Soliton Dynamics in Two-Dimensional van der Waals Interfaces. *Nano Lett.* **2020**, *20*, 1201–1207.
- (61) Telling, R. H.; Heggie, M. I. Stacking fault and dislocation glide on the basal plane of graphite. *Philos. Mag. Lett.* **2003**, *83*, 411–421.

- (62) Mele, E. J. Commensuration and interlayer coherence in twisted bilayer graphene. *Phys. Rev. B: Condens. Matter Mater. Phys.* **2010**, *81*, 161405.
- (63) Kim, K.; Coh, S.; Tan, L. Z.; Regan, W.; Yuk, J. M.; Chatterjee, E.; Crommie, M. F.; Cohen, M. L.; Louie, S. G.; Zettl, A. Raman Spectroscopy Study of Rotated Double-Layer Graphene: Misorientation-Angle Dependence of Electronic Structure. *Phys. Rev. Lett.* **2012**, *108*, 246103.
- (64) Barton, R. A.; Storch, I. R.; Adiga, V. P.; Sakakibara, R.; Cipriany, B. R.; Ilic, B.; Wang, S. P.; Ong, P.; McEuen, P. L.; Parpia, J. M.; Craighead, H. G. Photothermal Self-Oscillation and Laser Cooling of Graphene Optomechanical Systems. *Nano Lett.* **2012**, 12, 4681–4686.
- (65) Kim, S.; Yu, J.; van der Zande, A. M. Nano-electromechanical Drumhead Resonators from Two-Dimensional Material Bimorphs. *Nano Lett.* **2018**, *18*, 6686–6695.
- (66) Jia, H.; Yang, R.; Nguyen, A. E.; Alvillar, S. N.; Empante, T.; Bartels, L.; Feng, P. X.-L. Large-scale arrays of single- and few-layer MoS2 nanomechanical resonators. *Nanoscale* **2016**, *8*, 10677–10685.
- (67) Ye, F.; Islam, A.; Zhang, T.; Feng, P. X.-L. Ultrawide Frequency Tuning of Atomic Layer van der Waals Heterostructure Electromechanical Resonators. *Nano Lett.* **2021**, *21*, 5508–5515.
- (68) Barton, R. A.; Ilic, B.; van der Zande, A. M.; Whitney, W. S.; McEuen, P. L.; Parpia, J. M.; Craighead, H. G. High, Size-Dependent Quality Factor in an Array of Graphene Mechanical Resonators. *Nano Lett.* **2011**, *11*, 1232–1236.
- (69) Kramer, E.; van Dorp, J.; van Leeuwen, R.; Venstra, W. J. Strain-dependent damping in nanomechanical resonators from thin MoS2 crystals. *Appl. Phys. Lett.* **2015**, *107*, 091903.
- (70) de Silva, C. Vibration and Shock Handbook; Mechanical and Aerospace Engineering Series; CRC Press, 2005.
- (71) Mathis, A. T.; Balaji, N. N.; Kuether, R. J.; Brink, A. R.; Brake, M. R.; Quinn, D. D. A review of damping models for structures with mechanical joints. *Appl. Mech. Rev.* **2020**, *72* (4), 040802.
- (72) Koren, E.; Lörtscher, E.; Rawlings, C.; Knoll, A. W.; Duerig, U. Adhesion and friction in mesoscopic graphite contacts. *Science* **2015**, 348, 679–683.